Clays and Clay Minerals, Vol. 51, No. 6, 675–688, 2003.

ALTERATION OF VOLCANIC ROCKS AND GENESIS OF KAOLIN DEPOSITS IN THE ŞILE REGION, NORTHERN ISTANBUL, TURKEY. I: CLAY MINERALOGY

O. Isik Ece[1,2,*], Zenbe-E Nakagawa[2] and Paul A. Schroeder[3]

[1] Istanbul Technical University, Faculty of Mines, Mineralogy-Petrography Division, Maslak 80626 Istanbul, Turkey
[2] Akita University, Research Institute of Materials and Resources, Faculty of Engineering and Resources Science, Tegatagakuen-Cho, Akita 010-8502, Japan
[3] University of Georgia, Department of Geology, Athens, GA 30602-2501, USA

Abstract—The Şile Region contains discontinuous, cyclic, thin coal beds and industrial clay deposits that were accumulated in lacustrine basins which received extensive volcanoclastic sediments due to transport of highly weathered calc-alkaline volcanic rocks. The Sülüklü area has the largest kaolin deposit in this region. Cyclic kaolinization depended on the degree of leaching of Si and alkalis in cyclic swamp environments and, therefore, kaolinite contents vary in each discontinuous lens-shaped clay bed and underclay within the basin. The kaolins comprise disordered kaolinite, illite, smectite, gibbsite, quartz, pyrite, anatase, K-feldspar and goethite. Depth-related changes in the distribution of clay minerals, associated with coal beds, are indicative of organic acid-mineral reactions. Kaolinite crystallization initiated at the edges of sericitic mica sheets in the form of composite kaolinite stacks. The small size (<1 μm), morphology and poor crystallinity of kaolinite crystals suggest that kaolinization post dated transportation. Primary or secondary origins of particles can be determined from the stacking sequences of kaolinite particles using high-resolution transmission electron microscopy images. Kaolinite stacks always contain a small amount of illite, but smectite is only present in the middle and upper levels. Gibbsite is a main constituent of refractory bauxitic clays locally found as discontinuous lenses and exploited from the lower level of the basin.

Genesis of kaolin deposits took place in two stages: first, there was *in situ* weathering of the oldest andesitic agglomerates, tuffs and ashes at the base of the lacustrine basin coupled with discharge of shallow thermal waters which were initiated by local hydrothermal alteration; second, surface weathering enhanced transportation of altered rocks from the surrounding hills into the lacustrine basin. Kaolinization took place in cyclic swamp environments, as indicated by the presence of cyclic thin- to thick-bedded coals that provided necessary humic and fulvic acids for the post-depositional alteration of altered volcanic rocks to kaolin in dysaerobic, relatively low-pH conditions in saturated groundwater zones.

Key Words—Andesitic Suite, Coal Beds, DTA, Dysaerobic, FTIR, Kaolinite, Lacustrine Basin, SEM, TEM, Weathering.

INTRODUCTION

Kaolinite-rich deposits in coal-bearing strata along the western Black Sea coast have been studied because of their economic importance and their potential for recording the regional geological history (LoughNan, 1978). These cyclic alternating kaolin/coal beds are thought to have formed throughout the Oligocene-Miocene in swamp and lake environments in response to waxing and waning paleoclimatic conditions and variable regional tectonic uplift rates (Yeniyol and Ercan, 1989). Kaolin deposits found in the Şile region (Figure 1) formed in the presence of organic acids are similar to cyclic ball clay-coal beds of western Kentucky-Tennessee-Alabama sedimentary kaolin belts reported by Patterson and Murray (1984). Sediments accumulated in Oligocene delta plain and swamp environments, formed along what is now the northwest (European) Black Sea coastal region, are preserved as lignites. Lower Miocene lacustrine basin and swamp deposits are now found in the northeast (Asian) Black Sea coastal region near Istanbul, Turkey (Yeniyol, 1984).

The largest clay deposits occur in the Sülüklü area, on the Asian side of northern Istanbul. This Upper Miocene lacustrine sedimentary unit unconformably overlies weathered tuffs and ashes that belong to the Upper Cretaceous andesitic suite of the Western Pontides (Tüysüz, 1999; Yilmaz *et al.*, 1997). These altered volcanic rocks contain kaolinite, smectite and illite. This juxtaposition of the swampy, organic-rich basins next to a source of weathered volcanic rocks provides a unique opportunity to study the factors important to the formation of sedimentary-hosted kaolin deposits (*i.e.* kaolinite-rich deposits formed from *in situ* alteration of initially kaolinite-poor rocks). The purpose of this study is to examine the mineralogical and chemical characteristics of kaolins in the Sülüklü area in the context of models for the genesis of kaolin deposits.

* E-mail address of corresponding author:
ece@itu.edu.tr
DOI: 10.1346/CCMN.2003.0510610

GEOLOGICAL SETTING AND SAMPLING OF THE STUDY AREA

The Şile Region is situated in the northeast part of the Anatolian coast, east of Istanbul (Figure 1). The basement rocks of the Anatolian side of the Bosphorous–Istanbul Strait consist of Silurian conglomerate and sandstone beds with purple arkose units (sometimes gray to white) and Ordovician quartzites (Okay, 1948; Baykal and Kaya, 1965; Kaya, 1973, 1978). Lower–Middle Devonian rocks are represented by black biomicritic and biosparitic limestones, gradually grading upward to graywacke-schists, which are unconfomably underlain by the Silurian rocks (Abdülselamoğlu, 1963; Kaya, 1971, 1973).

A generalized stratigraphic section of the Şile region is given in Figure 2. The Lower Miocene kaolins generally form thick lenses occurring within relatively unconsolidated sands. Six thin coal seams are found in the middle and upper layers of the stratigraphic, section, occurring cyclically within cross-bedded sands (up to 10 m thick). There are three major coal-peat seams (80–150 cm) in the Şile region and many thin seams with variable thickness (5–25 cm). These seams overlie gray-beige to greenish underclays that are 0.4 to 1 m thick. The kaolin beds are 1.5 to 5 m thick and extend laterally up to 300 m. Bauxitic clays are discontinuously distributed and more abundant at the base of the section. Siderite is sporadically found in the base, suggesting a lack of marine-influenced sulfate reduction during the early diagenetic stages of the lacustrine basin and a lack of sulfur input from fault zones during deformation stages.

Kaolin reserves for the Sülüklü quarry are estimated to be ~50 million tons and it is the biggest deposit in the Şile Region. The average thickness of Sülüklü quarry is ~50 m (Figure 3). Correlation of the beds between subsurface boreholes is difficult because of the discontinuous nature of the lens-shaped clay beds and the wide spacing between core sites. The core data are therefore not directly shown in specific correlation with the quarry section shown in Figure 3.

The Şile region has been highly eroded and the present-day topography is relatively smooth. There are many small kaolin deposits associated with cyclic thin lignite beds. All altered volcanic rocks outside the basin are rich in smectite and illite, but no kaolinite is found. Two types of kaolinization are observed in the field site. The first includes the formation of residual kaolinite in weathered andesitic rocks. This kaolinite formed during primary weathering cycles and was later buried by Miocene lacustrine sediments in the basin. Residual kaolinites are found in saprolite zones along irregularly shaped bottom paleo-topography. This zone is exposed in only one area of the quarry due to mining activities. The second includes kaolinite found in the sediment-hosted kaolin deposits. We propose that these deposits were formed after the transport and deposition of

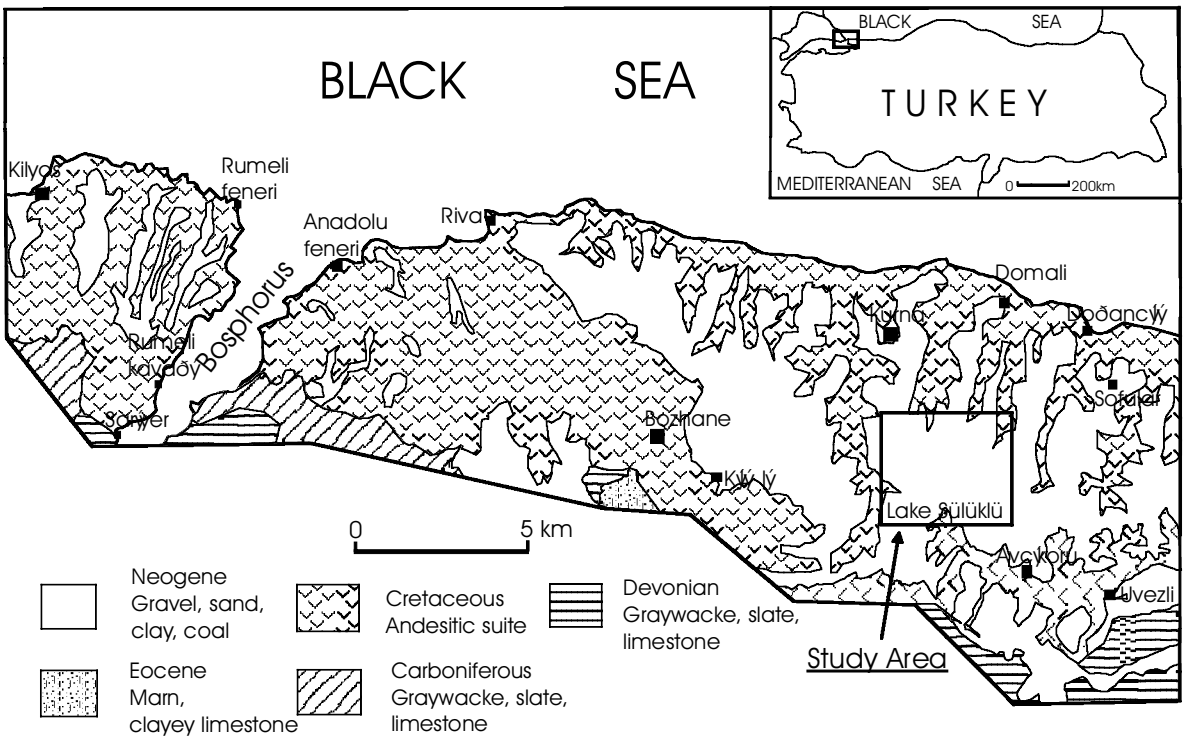

Figure 1. Index map of the study area.

https://doi.org/10.1346/CCMN.2003.0510610 Published online by Cambridge University Press

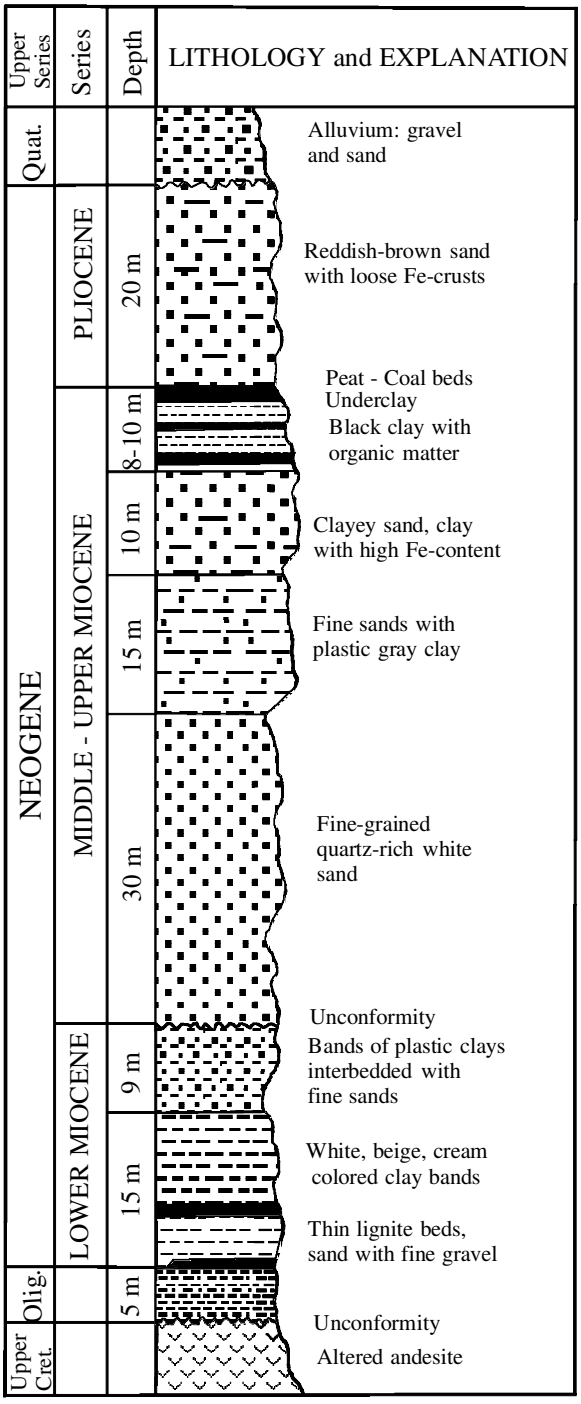

Figure 2. Generalized stratigraphic section of the Şile region (Özdamar, 1998).

sediments derived from the surrounding andesitic rocks. The large volume of fluvial sand beds in the upper level of sedimentary sequence were likely derived from the weathering of Cavuşbası granite, located ~15–20 km southwest of the study area.

MATERIALS AND METHODS

Clay samples were collected from the high walls of KaleMaden open clay quarries in the Sülüklü area. Core samples were also taken from the same deposit, and sampled at three intervals to 32 m depth. These are designated 99/558, 99/559 and 99/560, and represent kaolins layers from the top, middle and bottom parts of the section, respectively. The clay mineralogy was determined after size separation of the <2 μm size-fractions using standard centrifugation techniques (Hathaway, 1956). Bulk and clay mineralogy was examined by X-ray diffraction (XRD) using a RIGAKU, DMAX-2000 model X-ray powder diffractometer. The separated clay fractions were smeared on glass slides and dried. The clays were saturated with ethylene glycol vapor at 65ºC for 24 h to test for the presence of smectite.

Samples were also examined to determine the degree of structural disorder of kaolinite. The intercalation of dimethylsulfoxide (DMSO) technique (Thompson and Cuff, 1985) was used on oriented <2 μm fractions. Samples were also saturated with 100% hydrazine monohydrate ($NH_2NH_2.H_2O$) for 48 h at 70º and 90ºC, respectively, before XRD analyses. The approximate yield of intercalation for both techniques is estimated on the basis of the intensity ratio $\{I_{001\ treated}/(I_{001\ treated} + I_{001\ natural\ kaolinite})\}$ of Weiss *et al.* (1963). The larger the intensity ratio, the greater degree of disorder.

Differential thermal and thermogravimetric analyses (DTA/TG) of the <2 μm fractions were carried out with a Seiko SSC/5200 DTA/TG instrument under air. Samples were heated to 1000ºC at a rate of 10ºC/min. Infrared (IR) spectroscopic analyses were performed on pressed powders mixed with KBr (2 mg of <2 μm sample diluted by 200 mg KBr) using a Jasco 5300 FTIR spectrometer. Data were collected over the range 400–4000 cm^{-1}.

Micromorphological and textural features of various clays from the core samples were examined using a JEOL, JSM 890 scanning electron microscope (SEM). Small broken chip samples were coated with Pt-Au alloy. The relationship between particle-size distribution and morphology was studied with a HITACHI, HF-2000 high-resolution transmission electron microscope (HRTEM). The TEM clay slurries were prepared by dilution in distilled water and dispersion in an ultrasonic bath for 10 min. Pure carbon foil-covered polymer micro-grids were plunged into the clay slurry and dried on a hot plate for HRTEM examination.

The major elements of selected samples were determined with a RIGAKU 3070 X-ray fluorescence (XRF) spectrometer using the rock standards of the Geological Survey of Japan. 0.6 g of ground sample were fused with 6 g of a 4:1 mix of lithium metaborate and lithium tetraborate, for 20 min at 1100ºC, with intermittent swirling to ensure thorough mixing. The

https://doi.org/10.1346/CCMN.2003.0510610 Published online by Cambridge University Press

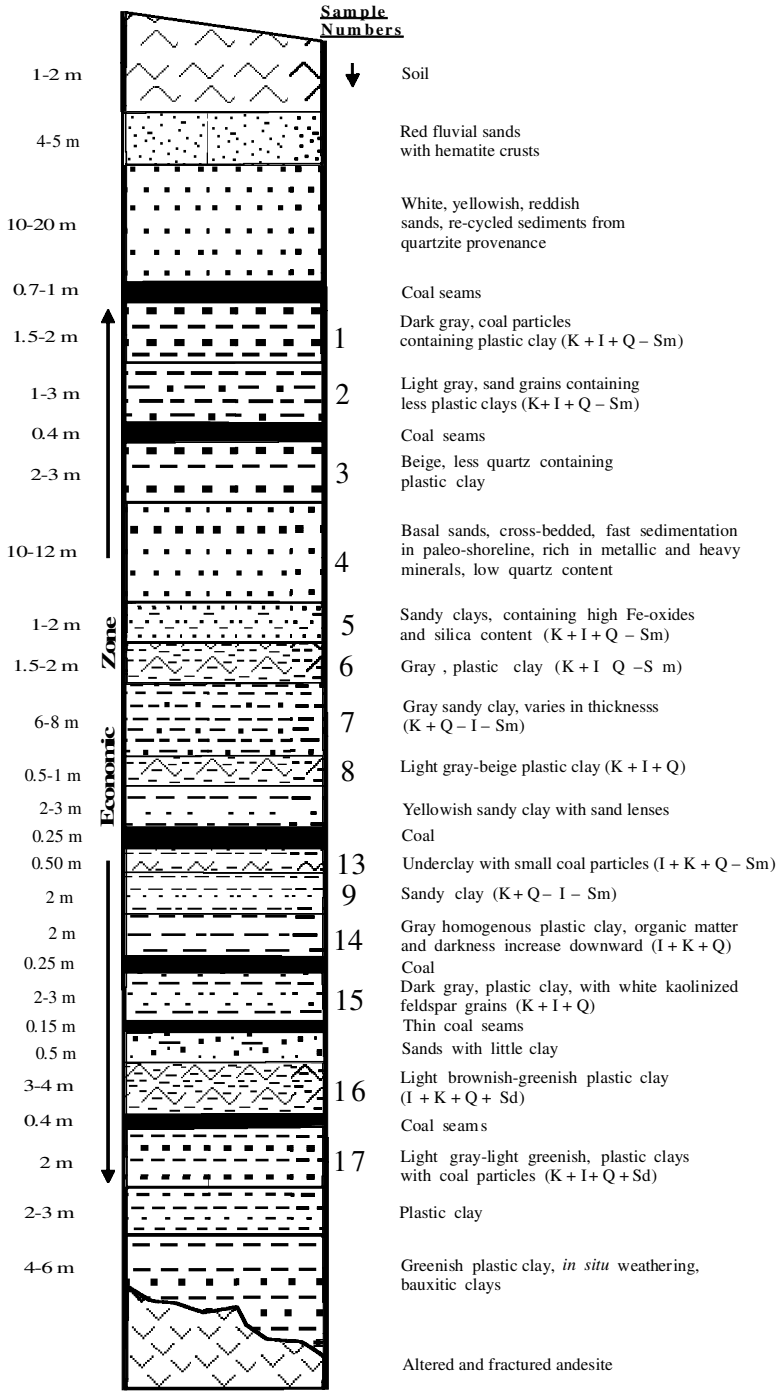

Figure 3. Stratigraphic section of Sülüklü clay quarry. K = kaolinite, I = illite, Q = quartz, Sm = smectite and Sd = siderite.

resultant melt was poured into (80% Pt + 20% Zr) molds to form glass beads. Some additional samples were analyzed for major elements (except Si) using a Perkin-Elmer 3030 model atomic absorption spectrometer (AAS). The samples were dissolved by acid digestion. The Si in the samples was determined using gravimetric methods.

MINERALOGY

XRD results

Disordered kaolinite, dioctahedral smectite, illite, K-feldspar, plagioclase, gibbsite, calcite, goethite, hematite and quartz were detected in all deposits. Trace amounts of pyrite, marcasite, anatase and organic matter are present in delta plain subfacies of the

https://doi.org/10.1346/CCMN.2003.0510610 Published online by Cambridge University Press

lacustrine environments. In the quarry, the discontinuous thin coal beds contain plastic, light-colored clays occurring in 50–200 m long and 1.5–3 m thick lens-shaped underclay zones. Underclays contain kaolinite, illite, smectite and mixed-layer illite-smectite.

Kaolinite is the main clay mineral present in all deposits (Figure 4). Kaolinite disorder was assessed using XRD peak full-widths at half-maximum (FWHM) of the 7.2 Å 001 reflection and the peak intensity of the 4.45 Å 020 reflection of the <2 μm fraction in the air-dried state (Table 1). The FWHM values range from 0.35º99/660), 0.45º (99/659) and 0.87º2θ CuKα (99/658). Feldspars (both plagioclase and K-feldspar) are present as minor phases. The XRD patterns indicate a trend of increasing kaolinite content with increasing depth in the stratigraphic section.

The DMSO results are only for the three representative top, middle and bottom samples from the kaolinite-

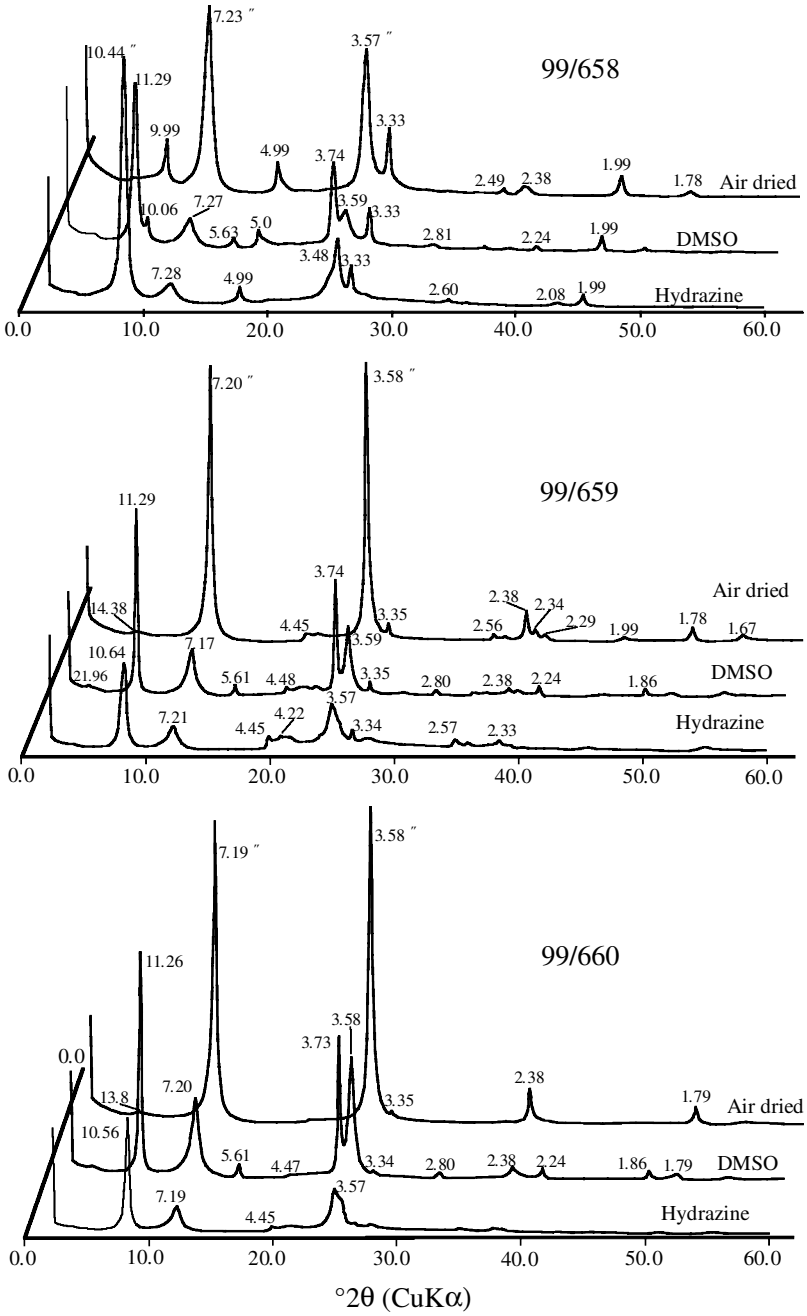

Figure 4. XRD patterns of oriented kaolinite samples. Only one sample (99/658) contains a small amount of illite and all samples contain a lesser amount of smectite.

https://doi.org/10.1346/CCMN.2003.0510610 Published online by Cambridge University Press

rich core zone. The results from DMSO and hydrazine monohydrate treatments are shown in Figure 4. Peak shifts of the kaolinite 001 reflection due to intercalation with DMSO can be used to differentiate kaolinite from non-expanding chlorite and serpentine-group minerals (Thompson and Cuff, 1985). Upon treatment with DMSO, the intensity of the basal reflections diminishes and the d_{001} peak migrates from 7.2 Å to a range between 11.26 and 11.29 Å. Basal reflections for hydrazine-treated samples diminish more than reflections of the DSMO-treated samples and the peak migrates to 10.5 Å. Lim *et al.* (1981) attributed these changes in peak intensity and position to crystal breakage and misorientation. When smectite is present, the 001 reflection shifts from 14.38 Å for the air-dried state to 21.96 Å after DMSO treatment (Figure 4b).

A small amount of kaolinite did not intercalate after the two-day treatment with DMSO. This is illustrated in Figure 4 by the presence of a 7.2 Å phase in all the treated samples. This 7.2 Å peak is probably not attributed to trioctahedral phases, because their presence would be indicated by a higher-order 004 reflection at 3.54 Å, and this is not seen (Costanzo *et al.*, 1984; Calvert, 1984). Using the method of Weiss *et al.* (1963), the intercalation ratios for DMSO are 85% (99/658), 80% (99/659) and 74% (99/660) and for hydrazine monohydrate are 92%, 79% and 81%, respectively (Figure 4). The DMSO ratio values reported here are slightly lower than the values reported for synthetic kaolinites by Satokawa *et al.* (1997), suggesting that our samples, although generally disordered, are slightly more well ordered than their synthetic counterparts.

DTA-TG results

Kaolin minerals are characterized by two major endothermic peaks and one exothermic peak. The exothermic peak corresponds to the destruction of the kaolinite 1:1 structure and is typically observed between 943 and 968ºC (Mackenzie, 1970). The dehydroxylation temperature of most kaolinites ranges from 498 to 514ºC, whereas the dehydroxylation of dickite and nacrite occurs at 680ºC. Well ordered kaolinite-T_c has an endothermic peak at ~580ºC, which is higher than the endothermic peak of 565ºC for kaolinite-M_d. Halloysite yields wide endothermic curves due to removal of intercalated water. Halloysite's main endothermic peak occurs at ~560ºC. The small differences in maximum temperatures for endothermic peaks for kaolin minerals is probably due to the small variations in chemistry and crystallinity relative to all other clay mineral groups (*e.g.* smectites).

Major weight losses during TG experiments occur between 400 and 600ºC. Additional weight losses (between 13.8 and 14.3 wt.%) occur at 943–968ºC (Figure 5). These values are in agreement with the LOI data (Table 1). The Şile disordered kaolinites (Figure 5) display average endothermic (513ºC) and exothermic (967ºC) events at lower temperatures than other kaolinites (Mackenzie, 1970). Holdridge and Vaughan (1957) showed that kaolinite endothermic peaks typically have maximum values near 550–600ºC. Keller *et al.* (1966) reported that the well crystallized Keokuk geode kaolinite gives a broad endothermic peak near 600ºC and they considered that the lower dehydroxylation temperatures of typical kaolinites can be attributed to inferior ordering and crystallinity, plus some effects from the small crystal size. The very small crystal size and poor crystallinity of our samples are likely to be the reason for low endothermic temperatures.

The slope ratio method, as defined by Robertson *et al.* (1954), is a sensitive way to detect differences in the shapes of DTA curves. Slope ratio is defined by the ratio of the angles (α and β) made between a vertical line at the peak maximum and the tangents to the left and right limbs of the peak (Figure 5). This method enables a numeric value to the symmetry of the peak, which can

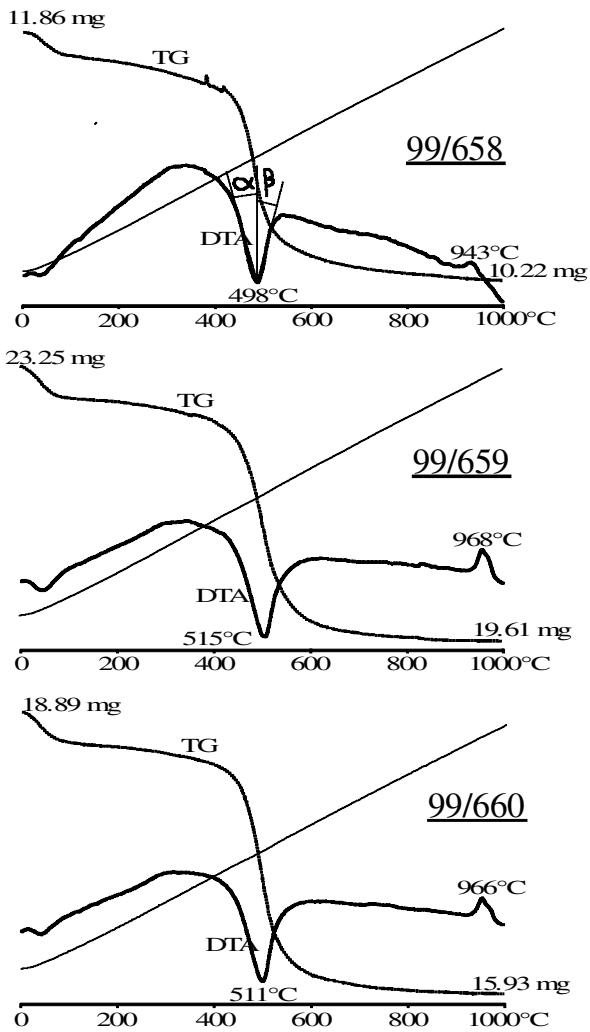

Figure 5. Representative DTA curves of kaolinites from the <2 μm size-fractions.

https://doi.org/10.1346/CCMN.2003.0510610 Published online by Cambridge University Press

Table 1. Disordering properties of kaolinites.

Sample no.	FWHM °2θ	d_{001}/d_{020}	d_{002}/d_{001}	LOI*	Water loss in DTA	DTA (C°)	FTIR DI**
99/658	0.87	6.5	0.788	–	14.08	498	0.71
99/659	0.45	32	~1	13.92	13.9	515	0.97
99/660	0.35	55	>1	13.75	14.3	511	0.89

* LOI = loss on ignition
** DI = disorder index (Muller and Bocquier, 1985)

differ for each mineral of the kaolin subgroup. Slope ratios of 0.8–1.0 for kaolinite-T_c, 1.2–1.4 for kaolinite-M_d and >1.8 for halloysite were measured by Robertson *et al.* (1954). The slope ratio values for our kaolinites are 1.38 for sample 99/658, 1.41 for 99/659 and 1.49 for 99/660. These values are similar to disordered kaolinite-M_d.

IR results

The IR studies were chosen because the stretching frequency of the OH bands in kaolin minerals display four sharp stretching bands between 3600 and 3700 cm^{-1} (Farmer, 1964). The strong band of 3697 cm^{-1} arises from surface hydroxyls and produces an in-phase vibration that is quasi-perpendicular to the 1:1 layers. Two other bands at 3670 and 3652 cm^{-1} arise from stretching vibrations that are sub-parallel to the 1:1 layers. The lowest frequency 3620 cm^{-1} band has been assigned to the fourth inner OH group (Giese, 1988). These spectral features can change due to the reorientation of OH groups in response to structural stresses. It is generally accepted that the band near 3619 cm^{-1} arises from internal OH groups and that near 3694 cm^{-1} arises from internal surface OH groups, and the doublet is characteristic of the kaolin subgroup. The 3620 and 3693 cm^{-1} bands are essentially unchanged, the existence of 3676 and 3650 cm^{-1} bands suggest an increase in ordering of kaolinite (Figure 2.4d in Russell and Fraser, 1995). They explained that the gradual reduction in size of the 3676 cm^{-1} band and broading of the 3650 cm^{-1} band are typical of disordered kaolinites. The disordering properties of kaolinite samples are shown in Table 1.

Figure 6 shows the IR spectra for the three samples 99/658, 99/659 and 99/660. An IR disorder index (DI), defined as I (3675 cm^{-1})/I (3650 cm^{-1}) helps to identify disordering in kaolinites (Muller and Bocquier, 1985). Disorder indices were calculated using absorbance units (A = –log (%T/100), thus allowing linear quantification of peaks (Schroeder, 2002). The DI values decrease with decreasing degree of order (Cases *et al.*, 1982) and are 0.71, 0.97 and 0.89, respectively, for the samples above. The 3628 cm^{-1} band in sample 99/658 (Figure 6) is due to the presence of a small amount of $2M_1$-illite. The weak band in the region of 3555 to 3568 cm^{-1} arises from H bonding between surface OH groups and adsorbed water (Kodama and Oinuma, 1963). The weak 3600 cm^{-1} band was interpreted as arising from OH-stretching and bending vibrations of $AlFe^{3+}OH$ groupings resulting from Fe^{3+} for Al substitution in the tetrahedral sheet of the kaolinite structure (Mendelovici *et al.*, 1979).

Mineral textures

Studies by SEM reveal a range of clay mineral morphologies that can be classified according to their variations in shape and size into: (1) folded sericitic mica flakes, (2) coarse-grained kaolinite (~1 μm),

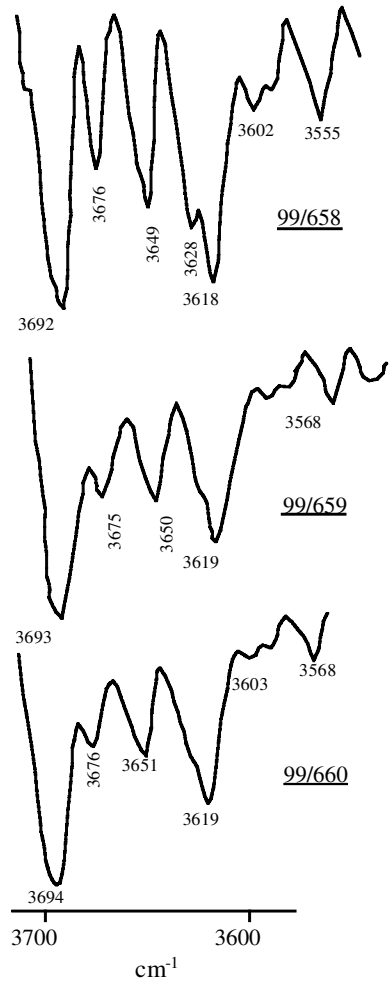

Figure 6. IR spectra of untreated kaolinites from the <2 μm size-fractions.

https://doi.org/10.1346/CCMN.2003.0510610 Published online by Cambridge University Press

(3) fine-grained kaolinite (~0.1 μm) (most common), and (4) rod-like tubular structures of halloysite, 0.1 μm in diameter and 1 to 1.5 μm in length (Figure 7). Almost all kaolinite samples studied exhibit irregular stacking of pseudohexagonal kaolinite platelets. Stacked particles formed by splitting of mica flakes are common

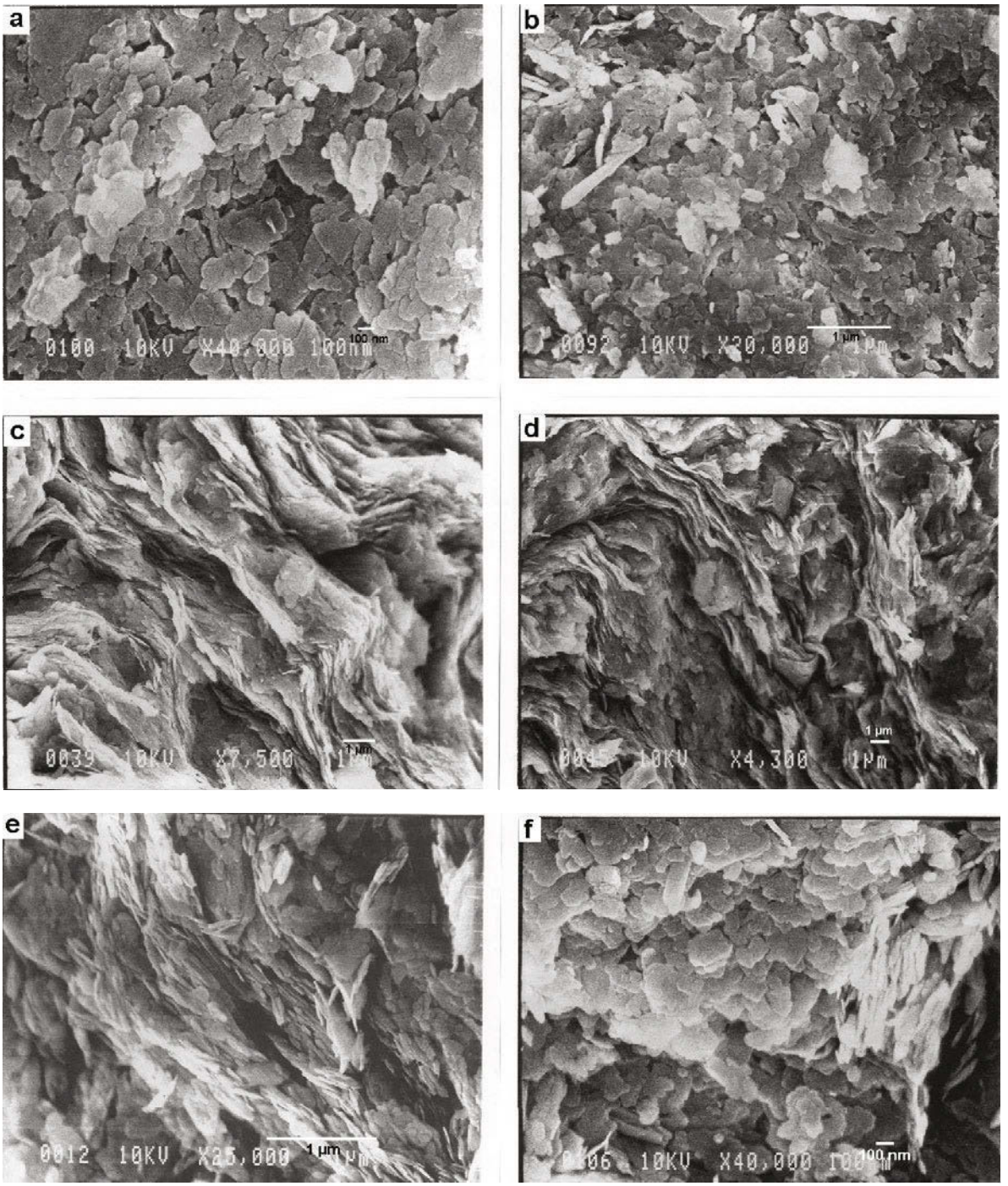

Figure 7. SEM images showing the textural relationship between sericite and poorly crystalline kaolinite/halloysite in the kaolin deposit studied: (a) stacking of 0.1–0.4 μm size kaolinite platelets; (b) kaolinite stacking with ~1 μm long acicular halloysite crystals; (c) kaolinite platelets forming at the expense of sericitic mica flakes; (d) under higher magnification, replacement of sericitic mica flakes by very fine size kaolinite particles; (e) kaolinite with thin, platy and very fine particles displaying shearing effects and delamination process; (f) stacking sequence of kaolinite and rare elongate halloysite crystals.

https://doi.org/10.1346/CCMN.2003.0510610 Published online by Cambridge University Press

(Figure 7a,b). The SEM studies indicate that kaolins consist of ultra-fine and thin platy particles and a lack of vermicular kaolinite books (Figure 7).

The kaolinite structure shows *c*-face centering on non-hydrogen atoms regardless of its origin and occurrence (Thompson *et al.*, 1989). The TEM studies also indicate that kaolinite particles have either thin (0.1–0.2 μm) and elongate (1.5 μm) shape (Figure 8a,b) or 1 μm wide flake morphology (Figure 8c,d,e). Figure 8f shows the presence of lattice fringes that are continuous across a number of layers in HRTEM images. Layer dislocation and lateral layer termination defects within layer stackings are observed in lattice-fringe images that are indicative of primary kaolinites, whereas deformations of the layers at the nano-scale (*i.e.* bending of several layers) are common in transported kaolinites (Ma and Eggleton, 1999). Cross-fringes indicate coherently stacked layers and stacking is ordered within these domains. The HRTEM images in Figure 8f display fringes from the kaolinite crystal, indicating the presence of primary kaolinite particles. In a limited number of samples, several sets of cross-fringes are examined, indicating the presence of secondary kaolinites.

GEOCHEMISTRY

The chemical analyses of the <2 μm size-fractions and structural formulae of representative kaolin samples are given in Table 2. Kaolinites, from the core samples have higher calculated tetrahedral Al contents than ideal kaolinite contents (Table 2). Most Fe_2O_3 and TiO_2 are attributed to oxides because the presence of free very fine-grained Fe oxide and anatase in sediment-hosted kaolins is very common (Weaver, 1976; Schroeder and Shiflet, 2000). Also, the SiO_2 contents of sample 99/659 in Table 2 and XRD data indicate the presence of clay-size quartz. In the core samples, the abundances of Ti and Fe are comparable suggesting diagenetic enrichment of Ti in kaolinite samples.

The major element contents of whole-rock samples are listed in Table 3. The Ti content increases slightly and the Fe, Mg and K contents decrease in the lower part of the quarry. The illite content as shown by the distribution of the K_2O content is greater in the upper and middle parts of the basin (Table 3). As shown in Table 3 (samples #16 and 17), the Fe_2O_3 and K_2O contents increase significantly and TiO_2 decreases slightly in residual kaolins at the base level of the open quarry, which shows dark greenish brown to dark greenish yellow color. Table 2 also shows that Ti, Fe and K decrease noticeably in <2 μm fractions below 28 m. In addition, the presence of a 2.4 wt.% Na_2O content in the clay fraction could be related to albite (Table 2). After exposure, the fresh clay surfaces change color to yellowish brown rapidly due to oxidation of pyrite at atmospheric conditions.

DISCUSSION

Lacustrine basins in the Şile Region are delineated by the structural depressions, which appear to be related to the intersection of extensional faults. In addition to tectonic events controlling the site of deposition, shallow

Table 2. Major element analyses (wt.%) of <2 μm clay size-fractions.

Sample no.	1	1-A	1B	1-C	2	2-A	3	5
SiO_2	48.98	43.12	48.32	45.38	56.64	43.5	47.76	51.08
Al_2O_3	32.52	35.18	32.79	34.92	26.81	33.25	32.74	30.59
TiO_2	1.37	0.95	1.34	1.19	1.27	0.98	1.22	1.24
Fe_2O_3	2.66	2.69	2.85	2.41	2.34	3.57	3.59	2.91
CaO	0.17	0.08	0.14	0.17	0.16	0.02	0.17	0.14
MgO	0.67	0.51	0.64	0.57	0.61	0.46	0.73	0.76
Na_2O	0.13	2.25	0.15	0.97	0.14	2.88	0.12	0.14
K_2O	2.81	2.36	2.61	2.18	2.55	2.16	2.42	2.65
LOI	11.18	11.53	11.47	12	8.96	11.35	11.71	10.24

Sample no.	6	6-A	7	8	9	99/213 (30 m)	99/659 (28 m)	99/660 (30 m)
SiO_2	50.01	44.36	46.44	42.93	41.88	48.9	46.79	43.56
Al_2O_3	31.7	31.97	34.07	36.69	36.11	33.75	36.4	36.65
TiO_2	1.13	0.92	1.19	0.91	0.91	0.607	0.908	0.864
Fe_2O_3	2.87	3.37	3.65	3.21	3.36	1.7	1.06	0.97
CaO	0.19	0.22	0.28	0.17	0.17	0.407	0.18	0.437
MgO	0.8	0.63	0.81	0.6	0.63	0.927	0.29	0.52
Na_2O	0.13	3.9	0.16	0.1	0.39	0.027	0.039	2.419
K_2O	2.8	2.31	2.16	1.74	1.71	0.417	0.152	0.436
LOI	10.08	10.03	11.81	13.68	14.7	12.87	13.92	13.75

https://doi.org/10.1346/CCMN.2003.0510610 Published online by Cambridge University Press

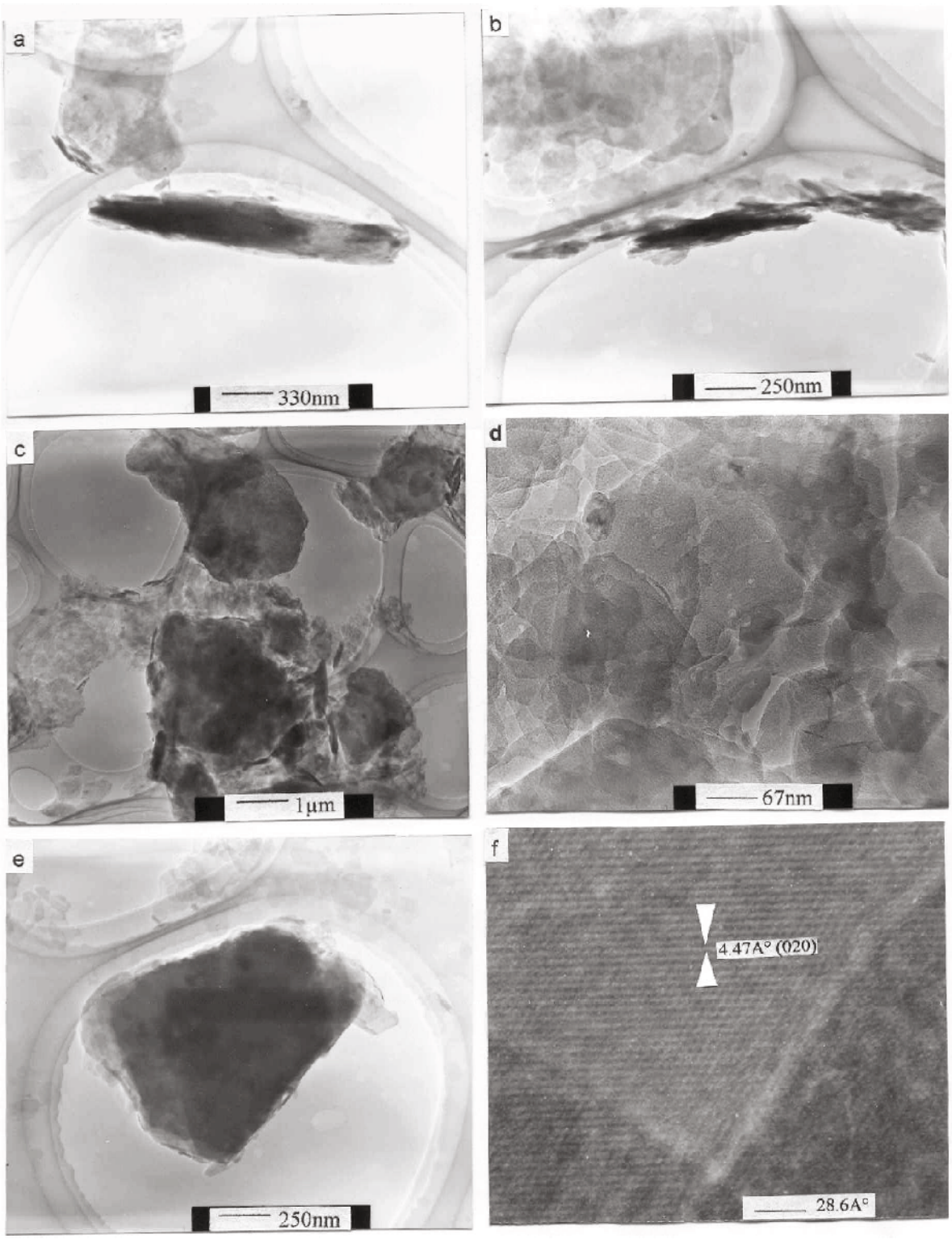

Figure 8. TEM images of kaolinite crystals showing very fine particles. (a) and (b) show the <1 μm size-fraction with elongate, possibly halloysite, crystals and fragmented flakes of sericites; (c) coexistence of kaolinite rouleaux, pseudohexagonal platelets, <0.5 μm elongate halloysite; (d) stacking of kaolinite platelets; (e) cluster of pseudohexagonal kaolinites; (f) defect-free interlayer fringes of kaolinite (020).

https://doi.org/10.1346/CCMN.2003.0510610 Published online by Cambridge University Press

Table 3. Major element analyses (wt.%) of bulk clay samples from Kalemaden quarry, Şile region. A, B and C refer to lateral sampling at the same interval.

Sample no.	1	1-A	1-B	1-C	2	2-A	2-B	3	5	6	6-A	7	8	9	14	15
SiO_2	63.99	65.21	60.86	55.39	64.05	71.4	68.26	56.82	73.2	55.25	59.4	48.84	47.41	55.15	64.26	61.93
Al_2O_3	22.48	21.78	24.45	28.43	22.02	8.11	19.48	26.84	16.59	28.07	24.69	32.15	33.56	27.71	21.45	23.69
TiO_2	1.19	1.19	1.15	1.11	1.2	0.57	1.21	1.07	1.08	1.11	1.18	1.16	1.1	1.01	1.2	1.3
Fe_2O_3	1.92	2.25	2.19	2.42	1.97	10.15	1.68	3.39	1.56	2.6	2.88	3.63	3.62	2.89	3.39	2.82
CaO	0.08	0.09	0.07	0.09	0.09	0.08	0.05	0.1	0.05	0.12	0.1	0.15	0.26	0.13	0.18	0.14
MgO	0.47	0.45	0.49	0.59	0.5	0.1	0.41	0.6	0.41	0.72	0.6	0.77	0.77	0.48	0.52	0.43
Na_2O	0.1	0.09	0.1	0.11	0.1	0.22	0.09	0.1	0.08	0.12	0.11	0.15	0.17	0.1	0.11	0.1
K_2O	2.18	2.11	2.29	2.43	2.28	0.75	1.92	2.13	1.61	2.7	2.47	2.13	2.05	1.56	2.25	1.9
LOI	7.03	7.14	8.09	9.38	6.77	8.61	5.82	8.88	4.68	8.66	7.82	11.35	10.47	10.95	6.68	7.74

Sample no.	16	17	99/211 10 m	99/212 26 m	99/213 30 m	99/641 4 m	99/642 9 m	99/643 14 m	99/644 18 m	99/645 19 m	99/656 20 m	99/657 22 m	99/658 24 m	99/659 28 m	99/660 30 m
SiO_2	55.07	46.63	61.89	56.85	60.29	61	63.02	58.5	54.35	57.74	50.32	61.83	59.06	58.94	62.64
Al_2O_3	24.76	31.23	23.67	26.73	25.8	23.6	22.63	24.43	28.12	23.1	23.92	23.79	25.42	28.4	25.4
TiO_2	0.98	0.83	1.16	1.3	0.91	1.15	1.18	1.19	1.18	1.11	0.84	1.15	1.14	1.53	1.94
Fe_2O_3	7.02	6.6	2.47	2.81	3.07	3.02	2.49	3.41	3.25	5.65	6.29	1.93	2.35	0.84	1.01
CaO	0.13	0.28	0.07	0.21	0.28	0.1	0.09	0.23	0.13	0.21	0.14	0.11	0.11	0.1	0.1
MgO	0.43	0.4	0.5	0.62	0.65	0.65	0.54	0.74	0.7	0.7	0.36	0.54	0.6	0.13	0.18
Na_2O	0.13	0.1	0.09	0.1	0.05	0.13	0.11	0.13	0.15	0.13	0.1	0.09	0.1	0.1	0.06
K_2O	2	0.47	2.12	2.11	0.21	2.48	1.9	2.62	2.47	2.45	1.62	2.58	2.69	0.12	0.01
LOI	9.54	13.51	7.13	8.65	9.46	7.26	7.28	8.29	9.09	7.98	16.39	7.14	7.9	9.87	9.2

thermal waters emerging from lower parts of the basin have also influenced the diagenetic history of the clays. The underlying andesitic volcanic rocks were altered by a high-temperature reaction with geothermal waters. These highly silicified altered volcanic rocks are mostly observed south of Sofular (Figure 1), and indicate the presence of multi-fracture systems within an andesitic suite. Coban *et al.* (2002) showed that the altered andesites contain abundant very fine silt-sized pyrite, which is indicative of SO_4^{2-} and/or HS^- input in the basin. During the final stage of hydrothermal alteration, favorable conditions for a period of low-temperature alteration and for the development of a basin drainage system, which was able to deliver clay- and silt-sized altered sediments into a shallow lacustrine basin. We postulate that these post-depositional conditions of alteration did not favor formation of well-ordered pseudo-hexagonal kaolinite, but were suitable for crystallization of halloysite and disordered kaolinite.

Exposures of *in situ* weathering of volcanics are found in the south of Sofular (Figure 1). Lower Cretaceous flysch sediments are overlain unconformably by Upper Cretaceous volcanic rocks of andesitic composition from base to top as follows; volcanic sandstones, tuffs and ashes, agglomerates and exfoliated volcanic rocks (concentric sheets). The alteration products of the incipient stage of hydrothermal alteration are smectite, illite and highly altered amorphous soft and poorly cemented volcanic tuffs and ashes in different proportions. All these altered units were affected by overprinted weathering processes; followed by young tectonic events and low-grade localized hydrothermal activities. No evidence for kaolinization is found in the weathered volcanic suite of the surrounding hills. The absence of kaolin minerals in the highland areas indicates that kaolinization is closely associated with thin coal beds and underclays in the basins. For this reason, the precursors of kaolinites are probably smectite, illite and altered feldspar. In the first stage, *in situ* weathering of andesitic volcanic rocks yielded smectite, which typically forms in alkaline and organic-poor conditions suggests basic waters were present at the time of clay formation. During a second stage, post-depositional kaolinization occurred at the expense of fine-grained altered volcanic rocks and smectites that were transported from surrounding hills into organic-rich-dysaerobic environments. Kaolinite formed in a Miocene shallow lacustrine basin as the result of chemical leaching of volcanic rocks in an organic-rich slightly acidic open system. Cyclic climatic effects followed by seasonal rains caused shifts in the delta channels and abandonment of channel segments, which favored the accumulation of clay deposits. The late-stage weathering of Cavuşbası granite provided sandy sediments and discontinuous lens-shaped sand beds indicative of fluvial sedimentation in the upper level of the basin. The presence of lens-shaped sand deposits overlying coal seams in the stratigraphic succession (Figure 3) indicates a fast fluvial sedimentation rate during cyclic episodes of the Plio-Quaternary period and multiple sources of terrestrial clays and sand deposits.

https://doi.org/10.1346/CCMN.2003.0510610 Published online by Cambridge University Press

It is more likely that halloysite formed *in situ* in the weathering profile at the base of the lacustrine basin because halloysite does not survive long-term distance transport. Large amounts of feldspar had been transported and altered from surrounding high lands to lacustrine basins by rivers. Some clay lenses contain small amounts of quartz sand in the upper part.

Hurst and Pickering (1997) suggested that the Georgia and South Carolina kaolins in the USA were produced, in part, by dysoxic weathering in saturated groundwater zones, but also by more oxic weathering in unsaturated zones, where bauxites also formed locally. The Şile kaolin deposits cover much smaller areas than the Georgia and South Carolina kaolin deposits and therefore the role of diagenetic pore-waters in a coal-forming lacustrine basin is more important than that of ground-waters. The Hurst and Pickering (1997) proposed mechanism for kaolinization is consistent with that of the Şile kaolins. The following post-depositional features in the Sülüklü kaolin deposit can be described. (1) Leaching of Na from the original rocks during formation of kaolins (Table 3, and also Table 1 in Ece and Nakagawa, 2003). Downward migration of Fe and Si; Na is leached away during extensive weathering of feldspar and K is partially consumed during the illitization of smectite. The enrichment of Ti and formation of anatase are important changes, especially in deepest core samples, below 28 m. (2) Local dissolution of kaolinite to form gibbsite in the lower part of the stratigraphic section; high Al (38–43 wt.%) bauxitic clays. These are known as 'refractory clays'; they occur sporadically in the basin and had been mined out in the past due to their commercial importance. The abundance of smectite decreases downward. (3) The gradual loss of smectite by groundwater leaching is a very slow process at low temperatures (Hurst and Pickering, 1997). (4) Pyrite is only found in coal and underclays. The early post-depositional changes began with the oxidation of pyrite to very thin Fe crust, as observed locally in the clay horizons. In addition, the presence of goethite is an indicator of bacterially mediated breakdown of pyrite which produces sulfuric acid (Evangelou, 1995), providing the low-pH conditions necessary for the formation of kaolin deposits in saturated ground-water zones. (5) Quarry outcrops display lateral transition of clay lenses in different length and thickness as depositional feature, suggesting shallow delta-plain subfacies.

The genesis of Şile kaolin deposits can be considered as similar to that of ball clays due to mineralogical composition and stratigraphic succession with cyclic coal seams. Similar ball clay occurrences have been reported from rather restricted geographic locations, such as Bavaria (Germany), Devon (England) and Kentucky and Tennessee (USA). Triassic altered arkosic sands in Bavaria have been kaolinized and the arkoses contain 75–85% quartz, ~10% kaolinite and the remainder consists of a partially kaolinized feldspar and a small amount of smectite and illite (Murray and Keller, 1993). The Cretaceous and Tertiary kaolin deposits of Middle Georgia were derived from granites and gneisses from the Piedmont. As discussed above, it has been proposed that post-depositional alteration and recrystallization produced the kaolin deposits (Hurst and Pickering, 1997). Also, trace element data support the concept that the fine-particle Tertiary kaolins in East Georgia have been derived from metavolcanic phyllites (Dowbrowski, 1993).

The South Carolina-Georgia-Alabama sedimentary kaolin belt extends for a distance of nearly 400 km. The Cretaceous beds consist of white, cross-bedded, irregular and channel-fill deposits of medium to coarse, rounded to angular quartz sands (Patterson and Murray, 1984). Interstitial kaolinitic clay, kaolin balls and white mica flakes are common in the sand. The Paleocene–Lower Eocene beds consist of cross-bedded, mostly medium-grained to very coarse-grained white sands, abundant channel fill deposits and contain scattered small lignitic and carbonaceous clay deposits; kaolin balls and rounded masses of pisolitic clay and bauxite occur locally. The Huber Formation in Georgia has lignitic clays containing Paleocene pollen and brown kaolin lenses rich in organic matter (Patterson and Murray, 1984). This description of Huber Formation indicates good correlation with Şile kaolin deposits in which cyclic coal beds are much thicker and more abundant.

The Minnesota sedimentary kaolin deposit formed by tropical weathering of altered of Precambrian metamorphic and igneous rocks and was deposited during early Late Cretaceous. Minnesota kaolin deposits, which extend for ~75 km, are composed primarily of kaolinite and are associated with natural gas-bearing organic matter-rich, silty shale beds (Patterson and Murray, 1984). The kaolin belt of the Western Kentucky–Tennessee region of Eocene age is the major source of ball clays, which occur in lenticular units containing sand, clay and lignite. Clay units range from 1 m to >5 m. Lignite and lignitic clays have discontinuous beds and lenticular units that overlie the ball clays.

All altered volcanic materials from the Şile Region, having undergone chemical leaching and precipitation, are transported into a peat-forming swamp environment resulting in the formation of coal seams. Fine-grained glassy materials and smectite group minerals dissolve and kaolinite precipitates if leached by large volumes of low-pH shallow ground-water containing humic and fulvic acids dissolved from above and below peats (Bohor and Triplehorn, 1993). This chemical alteration processes yield mainly kaolinite and hydrated silica and cations in solutions migrate from the system. The smectite content increases in the upper level of the basin because leaching was probably restricted or the abundance of organic acids in circulating waters was insufficient for mineral transformation.

CONCLUSIONS

The formation of large kaolin deposits is both associated with cyclic post-depositional alteration and cyclic swamp environments inside the basin. Crystal chemistry studies support a genetic model that includes (1) *in situ* weathering of volcanic tuffs, ashes and agglomerates, in which smectite commonly forms on the top of surrounding hills and no kaolinite is found outside the basin. (2) Andesitic volcanic rocks in the surrounding area were altered to smectite, which in turn was transported from multi sources in delta plain-swamp environments of lacustrine basin and were leached out to form kaolinite, amorphous silica and excess cations in solution in dysaerobic and low-pH conditions. (3) Dysaerobic weathering of highly altered andesitic rocks requires differential mobility of elements by the presence of humic and fulvic acids produced in the swamp environment, which leaches K^+ and other elements necessary for the crystallization of kaolinite. (4) The evolution of very fine-grained kaolinite is associated with sericitization of feldspar in late-stage alteration phenomena. (5) In addition, the Şile region is subject to relatively low annual temperature and high rainfall that have induced more intense weathering and regional groundwater movements in the shallow lacustrine basin. (6) Kaolinite–gibbsite transformation is associated with groundwater movement and the degree of weathering in permeable zones. Gibbsite formed in the lower horizon of the stratigraphic section as a result of dissolution of kaolinite during the late-stage weathering processes.

Titanium enrichment, as anatase, is observed in fine silt-sized fractions in a relatively deeper part of the basin. However, the chemical analyses showed that there is no significant difference in TiO_2 distributions between bulk clay samples and <2 μm clay-sized fractions in the upper and middle parts of the basin. The occasional presence of halloysite indicates that at least some kaolin was transported a relatively short distance; otherwise the halloysite crystals would have broken down because they would not have survived long-distance transport. Generally, the Fe and Ti contents of Şile kaolins are relatively high probably due to the diagenetic processes.

ACKNOWLEDGMENTS

We thank to Ms Saori Watanabe and Ms Kiko Okada of Akita Research Institute of Advanced Technology, Japan for providing the opportunity to carry out SEM and TEM studies. We would like to express our personal gratitude to Professors George Christidis and Andre Lalonde for their excellent review comments and suggestions. We also express our thank to Mustafa Bal of Kalemaden A.Ş. for his logistic and laboratory support during the field studies. This research is partly supported by ITU Research Fund (No: 775).

REFERENCES

Abdülselamoğlu, S. (1963) Istanbul boğaz doğusunda mostra veren Paleozoyik arazide stratigrafik ve paleontolojik yeni müşahedeler. *MTA Dergisi*, **60**, 1–7.

Baykal, F. and Kaya, O. (1965) İstanbul Siluryeni hakknda. *MTA Dergisi*, **64**, 1–8.

Bohor, B.F. and Triplehorn, D.M. (1993) Tonsteins: Altered volcanic ash layers in coal-bearing sequences. *Geological Society of America Special Paper*, **285**, 44 pp.

Calvert, C.S. (1984) Simplified, complete CsCl-hydrazine-dimethysulfoxide intercalataion of kaolinite. *Clays and Clay Minerals*, **32**, 125–130.

Cases, J.M., Lietard, O., Yvon, J. and Delon, J.F. (1982) Estude des propriétés cristallchimiques, morphologiques, superficielles de kaolinites désordonnés. *Bulletin de Mineralogié*, **105**, 439–455.

Çoban, F., Ece, Ö.I., Yavuz, O. and Özdamar, Ş. (2002) Petrogenesis of volcanic rocks and clay mineralogy and genesis of underclays, Şile Region, İstanbul, Turkey. *Neues Jahrbuch für Mineralogie Abhandlungen*, **178**, 1–25.

Costanzo, P.M., Giese, R.F., Jr and Clemency, C.V. (1984) Synthesis of a 10 Å hydrated kaolinite. *Clays and Clay Minerals*, **32**, 29–35.

Dowbrowski, T. (1993) Theories of origin for the Georgia kaolins: A review. Pp. 75–97 in: *Kaolin Genesis and Utilization* (H. Murray, W. Bundy and C. Harvey, editor). Special Publication **1**. The Clay Minerals Society, Bloomington, Indiana.

Ece, Ö.I. and Nakagawa, Z. (2003) Alteration of volcanic rocks and genesis of kaolin deposits in Şile Region, Northern İstanbul, Turkey. II: Differential mobility of elements. *Clay Minerals* (in press).

Evangelou, V.P. (1995) *Pyrite Oxidation and its Control*. CRC Press, New York, 293 pp.

Farmer, V.C. (1964) Infrared absorption of hydroxyl groups in kaolinite. *Science*, **145**, 1189–1190.

Giese, R.F. (1988) Kaolin minerals: structures and stabilities. Pp. 29–66 in: *Hydrous Phyllosilicates* (S.W. Bailey, editor). Reviews in Mineralogy **19**. Mineralogical Society of America, Washington, D.C.

Hathaway, J.C. (1956) Procedure for clay mineral analysis used in the sedimentary petrology laboratory of the U.S. Geological Survey. *Minerals Bulletin*, **3**, 8–13.

Holdridge, D.A. and Vaughan, F. (1957) The kaolin minerals. Pp. 224–286 in: *The Differential Thermal Investigations of Clays* (R.C. Mackenzie, editor). Monograph **2**. The Mineralogical Society, London.

Hurst, V. and Pickering, S. (1997) Origin and classification of Coastal Plain kaolins, Southwestern USA, and the role of groundwater and microbial action. *Clays and Clay Minerals*, **45**, 274–285.

Kaya, O. (1971) Istanbul'un Karbofiner stratigrafisi. *Türkiye Jeoloji Kurumu Bulteni*, **14/2**, 143–199.

Kaya, O. (1973) Paleozoic of Istanbul. *Ege Universitesi Fen Fakültesi Yayn*, **40**, 1–25.

Kaya, O. (1978) Istanbul Ordovisiyen ve Siluryeni. *Hacettepe Yerbilimleri Dergisi*, **4/1-2**, 1–22.

Keller, W.D., Pickett, E.E. and Reeman, A.L. (1966) Elevated hydroxyl temperature of the Keokuk geode kaolinite – a possible reference material. *Proceedings of the International Clay Conference, Jerusalem*, 75–85.

Kodama, H. and Oinuma, K. (1963) Identification of kaolin minerals in the presence of chlorite by X-ray diffraction and infrared absorption spectra. *Clays and Clay Minerals*, **11**, 236–249.

Lim, C.H., Jackson, M.L. and Higashi, T. (1981) Intercalation of soil clays with dimethysulfoxide. *Soil Science Society of America Journal*, **45**, 433–436.

Loughnan, F.C. (1978) Flint clays, tonsteins and the kaolinite clayrock facies. *Clay Minerals*, **13**, 387–400.

Ma, C. and Eggleton, R. (1999) Surface layer types of kaolinite: A high-resolution transmission electron micro-

scope study. *Clays and Clay Minerals*, **47**, 181–191.
Mackenzie, R.C. (1970) Simple phyllosilicates based on gibbsite- and brucite-like sheets. Pp. 498–537 in: *Differential Thermal Analysis* (R.C. Mackenzie, editor). Academic Press, London.
Mendelovici, E., Yaris, S. and Villalbor, R. (1979) Iron-bearing kaolinite in Venezuelan laterites. 1. Infrared spectroscopy and chemical dissolution evidence. *Clay Minerals*, **14**, 323–331.
Muller, J.-P. and Bocquier, G. (1985) Textural and mineralogical relationships between between ferruginous nodules and surrounding clayey matrices in a laterite from Cameroon. *Proceedings of the International Clay Conference*, *Denver*, pp. 186–194.
Murray, H.H. and Keller, W.D. (1993) Kaolins, kaolins and kaolins. Pp. 1–24 in: *Kaolin Genesis and Utilization* (H. Murray, W. Bundy and C. Harvey, editors). Special Publication **1**. The Clay Minerals Society, Bloomington, Indiana.
Okay, A.C. (1948) Şile, Mudarl, Kartal ve Riva arasndaki bölgenin jeolojik etüdü. *İstanbul Universitesi Fen Fakültesi Mecmuas*, **XIII/4**, 311–335.
Özdamar, S. (1998) Clay mineralogy of underclays in the Şile region, Istanbul, Türkiye. MSc thesis, Istanbul Technical University, 117 pp.
Patterson, S.H. and Murray, H.H. (1984) Kaolin, refractory clay, ball clay and halloysite in North America, Hawaii and the Caribbean region. *US Geological Survey Professional Paper*, **1306**, 56 pp.
Robertson, R.H.S., Brindley, G.W. and MacKenzie, R.C. (1954) Mineralogy of kaolin clays from Pugu, Tanganyika. *American Mineralogist*, **39**, 18–139.
Russell, J.D. and Fraser, A.R. (1995) Infrared methods. Pp. 11–67 in: *Clay Mineralogy* (M.J. Wilson, editor). Chapman & Hall, London.
Satokawa, S., Miyawaki, R., Tomura, S. and Shibasaki, Y. (1997) DMSO-Intercalation of synthetic kaolinites. *Clay Science*, **10**, 231–239.
Schroeder, P.A. (2002) Infrared spectroscopy in clay science. Pp. 182–206 in: *Teaching Clay Science* (A.C. Rule and S. Guggenheim, editors). CMS Workshop Lectures, **11**. Clay Minerals Society, Denver, Colorado.
Schroeder, P.A. and Shiflet, J. (2000) Ti-bearing phases in the Huber Formation, an east Georgia kaolin deposit. *Clays and Clay Minerals*, **48**, 151–158.
Thompson, J.G. and Cuff, C. (1985) Crystal structure of kaolinite: Dimethylsulfoxide intercalate. *Clays and Clay Minerals*, **33**, 490–500.
Thompson, L.G., FitzGerald, J.D. and Withers, R.L. (1989) Electron diffraction evidence for C-centering of non-hydrogen atoms in kaolinite. *Clays and Clay Minerals*, **37**, 563–565.
Tüysüz, O. (1999) Geology of the Cretaceous sedimentary basins of the Western Pontides. *Geological Journal*, **34**, 75–93.
Weaver, C.E. (1976) The nature of TiO_2 in kaolinite. *Clays and Clay Minerals*, **24**, 215–218.
Weiss, A., Thielepape, W., Goring, G., Ritter, W. and Schfer, H. (1963) Kaolinite intercalation compounds. *Proceedings of the International Clay Conference*, *Stockholm*, pp. 287–305.
Yeniyol, M. (1984) Istanbul killerinin olusumu (occurrence of clays of Istanbul). *Turkiye Jeoloji Kurumu Bulteni*, **5**, 143–150.
Yeniyol, M. and Ercan, T. (1989) Geology of the Northern İstanbul, petrochemical characteristics of Upper Cretaceous volcanism and its regional distribution in Pontides. *I.U. Yerbilimleri Dergisi*, **7**, 125–147.
Yılmaz, Y., Tüysüz, O. Yigitbaş, E. (1997) Geology and tectonic evolution of the Pontides. Pp. 183–226 in: *Regional and Petroleum Geology of the Black Sea and Surrounding Region.* AAPG Memoir **68**. American Association of Petroleum Geology.

(*Received 8 April 2002; revised 18 July 2003; Ms. 647*)